High Voltage

Research Article

IET Journals
The Institution of Engineering and Technology

Model to estimate the trapping parameters of cross-linked polyethylene cable peelings of different service years and their relationships with dc breakdown strengths

ISSN 2397-7264
Received on 6th May 2016
Revised on 8th June 2016
Accepted on 9th June 2016
doi: 10.1049/hve.2016.0012
www.ietdl.org

Ning Liu[1] ✉, Churui Zhou[1], George Chen[1], Yang Xu[2], Junzheng Cao[3], Haitian Wang[3]

[1]*Tony Davies High Voltage Laboratory, University of Southampton, Southampton, UK*
[2]*State Key Laboratory of Electrical Insulation and Power Equipment, Xi'an Jiaotong University, Xi'an, People's Republic of China*
[3]*State Grid Smart Grid Research Institute (SGRI), Beijing, People's Republic of China*
✉ *E-mail: nl4g12@soton.ac.uk*

Abstract: In this study, an improved trapping/detrapping model was used to simulate the charge dynamics in cross-linked polyethylene peelings from different-year aged cables. Injection barrier of trapping parameters was estimated by the model fitted to experimental data for each type of sample. Moreover, dc breakdown tests were operated on those samples. It has been found that the dc breakdown strength of inner-layer samples is the lowest in cable sections with thicker insulation layer taken from high-voltage ac (HVAC) 220 kV service condition, whereas for the cable with thinner insulation from HVAC 110 kV, middle-layer samples have worst breakdown performance. This might be explained by the space charge issues under long-term HVAC condition. More importantly, a clear relationship between estimated model parameters, including injection barrier, trap depth and trap density, with the dc breakdown strength in each layer has been reported in this study.

1 Introduction

During long-term operation of cross-linked polyethylene (XLPE) high-voltage (HV) cables, ageing process can cause the increase in amorphous region ratio, creation of more microvoids and discontinuities, chain scission, oxidation and hydrolysis. These will introduce more physical and chemical defects into the materials and lead to the rise of localised states residing within the wide bandgap. These localised states, or namely traps, with density N, offer charge carriers at an intermediate energy level, i.e. trap depth E_t. Meanwhile, the ability of these traps to capture charge carriers relates to the trapping cross-section area S. Assuming traps are Coulombic-attractive type and one trap site could only accommodate one charge carrier, thus the cross-section area could be calculated as $S=\pi r^2$, where r is the distance between the capturing site and its trapped charge. To summarise, trap density N, trap depth E_t and trapping cross-sectional area S are generally called trapping parameters, which depict the attributes of traps. In our research, we aim to take advantage of these attributes of 'traps' to monitor ageing for different-degree aged insulation materials.

In recent years, many approaches have been developed on determination or estimation of these trapping parameters for various insulation materials, especially polyethylene [1–5]. Chen proposed a trapping–detrapping model based on two energy levels [1]. Thereafter in [2, 3], by employing the charge detrapping part in the model established by Chen, trapping parameters of low-density polyethylene (LDPE) and also gamma-irradiated LDPE were estimated. It has been revealed that physical and chemical modifications brought by irradiation process could be reflected on the changes of trapping parameters. In the case of epoxy resin, Dissado *et al.* [4] proposed a model considering charge detrapping process within three steps. Furthermore, through such model, trapping parameters of different-time aged XLPE cable peelings [5] were evaluated. Similarly, changes in trapping parameters were reported existing between XLPE peelings in different conditions. The basic idea of these two approaches to estimate trapping parameters have something in common: (i) both numerical models are applied to the condition of charge relaxation after the removal of the external voltage; (ii) the trapping parameters were obtained by fitted curve of specific model parameters with experimental data from only the depolarisation tests, i.e. data from polarisation test were not exploited; (iii) observed charge decay after switching off power supply was thought to be caused by detrapping process, or in other words, any charges escaped from the trap sites were presumed to flow away instantly; (iv) both studies tried to separate traps with a range of energy levels into two equivalent levels [1] or ranges [4]. It is noteworthy in works based on Chen's model [1–3], the two energy levels, i.e. shallow and deep traps, have been reported relating with physical and chemical defects in polymeric materials, respectively.

In this paper, we proposed a new approach, which not only inherit some merits of previous two model works but also was improved from many aspects, to estimate the trapping parameters of insulation materials. In terms of inheritance, trapping parameters are also determined by optimum curve fitting results with experimental data and meanwhile charge decay data are still meaningful information to the data fitting process. Except for that, following previous works, the present model also classifies the whole traps as shallow and deep traps. More importantly, comparing with previous works, the new model in this paper was mainly improved in two aspects: (i) in addition to charge relaxation after turning off power supply, the preceding space charge accumulation process during voltage-on condition was included within the simulation works; (ii) observed space charges in the bulk were considered to be consisted of trapped charges and mobile charges, which refer to those free charges transporting between traps.

2 Brief description of the model

The model was initially proposed in our previous paper [6]. In this paper, the model will be briefly reviewed as follows.

In the improved model, the observed charges are no longer treated as trapped charges only but include a non-negligible amount of

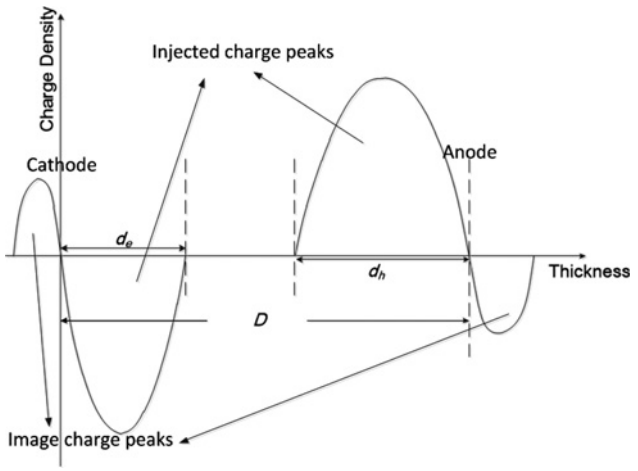

Fig. 1 *Space charge profile of homocharge injection denoted with separated charge region of positive and negative [6]*

mobile charges as well. Typically, space charge profile with homocharge injection could be divided as positive and negative charge region with thicknesses, respectively, equalling to d_h and d_e, as shown in Fig. 1. Therefore, the mean number density of net charges in either region can be calculated as

$$n_{h,e} = \frac{Q_{h,e}}{d_{h,e}A} \tag{1}$$

where $Q_{h,e}$ is the total charge amount in either charge region and A is the electrode area. The density of net charge $n_{h,e}$ in either region equals to the sum of trapped charge and mobile charge density, i.e.

$$n_{h,e} = n_{t_{h,e}} + n_{m_{h,e}} \tag{2}$$

where n_t and n_m represent trapped and mobile charge density, respectively, in either positive (n_{t_h} and n_{m_h}) or negative charge zone (n_{t_e} and n_{m_e}).

For the sake of convenience, the present model does not consider the charge movement inside the charge region. Instead, charges in the region will be integrated along the thickness d_h or d_e as an entirety.

2.1 Based on single energy level traps

To assist in establishing the improved model in which new features are introduced, we start with single energy level of traps in the material. The concepts are then extended to the two energy levels of trapping/detrapping processes.

2.1.1 Voltage-on condition: Here, an assumption has been made that the energy depth of all the traps is on the same level. For instance, in positive charge region, the changing rate for the injected net charge density n_h under external applied field E_a can be proposed as

$$\frac{dn_h}{dt} = \frac{J_h}{qd_h} - P_h n_{m_h} - \Delta n'_{m_e} \tag{3}$$

For the first term on the right side of (3), it represents the increasing rate of number volumic density of holes coming from the anode by injection. J_h is injection current density from the anode. With HV applied, charge injection behaviour at the metal–insulator interface was verified conforming to Schottky injection mechanism [7, 8], which has already been applied into some previous modelling works on polyethylene [9, 10]. If the electric field at the interface is E_{i_+}(at the anode, or E_{i_-} at the cathode), the injection current density J_h at the interface between the anode and dielectric can be found as [11]

$$J_h = A_0 T^2 \exp\left(-\frac{qw_h}{kT}\right) \exp\left(\beta_{sc} E_{i_+}^{0.5}\right) \tag{4}$$

where A_0 is the constant term, k is Boltzmann constant, T is temperature, ε_0 is the vacuum permittivity, ε_r is the relative permittivity for dielectric and w_h stands for the original injection barrier height holes (or w_e for electrons). Normally, Schottky constant is written as $\beta_{sc} = (q/kT)\sqrt{qE_{i+}/4\pi\varepsilon_0\varepsilon_r}$. When bipolar charges continuously inject into bulk, E_{i+} (or E_{i-}) will be modified. The calculation of E_{i+} (or E_{i-}) will not be shown in this paper due to the limitation of pages, and details can be found in our paper [6].

The second negative term on right side of (3) describes the decreasing rate of net charge in positive charge layer. Such reduction in the charge layer during voltage-stressing period should be the consequence of the outflow of holes from local charge region to the opposite electrode. Here, it is postulated that there is a fix portion P (s^{-1}) of mobile charges that will outflow from local charge region.

The third term $\Delta n'_{m_e}$ of (3) represents increasing rate of the mobile electrons existing in positive charge region, which are injected from cathode. To calculate these mobile charges in either space charge region, two situations have to be considered. At every moment, mobile holes of $P_h n_{m_h}$ shall flow from positive charge region to the other side of bulk meanwhile mobile electrons will flow from negative region towards the positive charge region with amount of $P_e n_{m_e}$.

If $P_h n_{m_h} > P_e n_{m_e}$, it can be thought that part of $P_h n_{m_h}$ will overlap with $P_e n_{m_e}$ in the flat region between negative layer and positive one, thus showing zero net charge in such region.

Residual positive mobile holes of $P_h n_{m_h} - P_e n_{m_e}$ will finally go to negative charge region, i.e. $\Delta n_{m_h} = P_h n_{m_h} - P_e n_{m_e}$ and $\Delta n'_{m_e} = 0$. Likewise, when $P_h n_{m_h} < P_e n_{m_e}$, mobile electrons of $P_e n_{m_e} - P_h n_{m_h}$ will flow to positive charge layer, i.e. $\Delta n'_{m_e} = P_e n_{m_e} - P_h n_{m_h}$, and $\Delta n'_{m_h} = 0$.

For the changing rate of positive trapped charge density n_{t_h}, it should consist of three segments, i.e.

$$\frac{dn_{t_h}}{dt} = -R_{esc} + R_{cap} - R_{rec} \tag{5}$$

where R_{esc} and R_{cap}, respectively, represent the charge escaping rate from the traps and charge capturing rate by traps [11]. R_{rec} is the recombination rate of trapped holes/electrons and mobile electrons/holes, which flow from the opposite charge region. Specifically, for positive charge layer, R_{esc}, R_{cap} and R_{rec} could be expressed as

$$R_{esc} = n_{t_h} \nu_0 \exp\left(-\frac{E'_{t_h}}{kT}\right) \tag{6}$$

$$R_{cap} = n_{m_h}\left(N_{t_h} - n_{t_h}\right) S_h \nu_{d_h} \tag{7}$$

$$R_{rec} = B\left(n'_{m_e}\right) n_t \tag{8}$$

In (6), ν_0 is the escape attempt frequency, E'_{t_h} is the modified trap depth based on original trap depth E_{t_h} with consideration of Poole–Frenkel lowering ΔV_{pf_h}

$$E'_{t_h} = E_{t_h} - \Delta V_{pf_h} \tag{9}$$

The energy barrier lowering ΔV_{pf_h} could be written in the form [11]

$$\Delta V_{pf_h} = \beta_{pf} E^{0.5} \tag{10}$$

where the Poole–Frenkel constant $\beta_{pf} = 2\beta_{sc}$.

High Volt., 2016, Vol. 1, Iss. 2, pp. 95–105

However, it was pointed out by several investigators that the Poole–Frenkel effect described by (10) is not dominant behaviour in bulk at high fields for polyethylene [7, 12, 13]. In accordance with (10) by plotting conductivity against the square root of electric field ($\sigma - E^{0.5}$), it will give a much higher relative permittivity value (14.2) for LDPE, than the true one (~2.2) [7]. Ieda *et al.* [14] proposed another corrected three-dimensional (3D) Poole–Frenkel model, which takes consideration of the angle θ between electric field E and electron (or hole)-trap distance r, and also an energy state δ lowering caused by electron/hole–phonon interaction. Such a model will fix the relative permittivity value of LDPE much closer to the true one [12, 13].

With such improved Poole–Frenkel model, the averaged barrier lowering considered 3D effect [14]

$$\Delta V_{\mathrm{pf_h}} = \frac{\int_0^{\pi/2} \beta_{\mathrm{pf}} (E\cos\theta)^{0.5}}{\pi/2} = 0.3814 \beta_{\mathrm{pf}} E^{0.5} \tag{11}$$

Meanwhile, considering increased barrier in the reverse direction of field, the equivalent barrier height lowering $\Delta V'_{\mathrm{pf_h}}$ could be found as

$$\Delta V'_{\mathrm{pf_h}} = kT \ln\left[2\cosh\left(\frac{\Delta V_{\mathrm{pf_h}}}{kT}\right)\right] \tag{12}$$

The full derivation of (11) and (12) will not be shown in this paper, but could be found in [6, 14].

In (7), the rate of charge capture R_{cap} by traps will be proportional to the density of mobile holes $n_{\mathrm{m_h}}$, unoccupied trap sites' density $N_{\mathrm{t_h}} - n_{\mathrm{t_h}}$, where $N_{\mathrm{t_h}}$ represents the total traps density for holes, and $v_{\mathrm{d_h}}$ is the drift velocity of charge carriers. Physically, such equation could be comprehended as: when mobile holes of density $n_{\mathrm{m_h}}$ move through the specimen with a velocity of $v_{\mathrm{d_h}}$, in Δt time, the free charges passing through empty traps of density $N_{\mathrm{t_h}} - n_{\mathrm{t_h}}$ with a cross-section area of S_{h} are $n_{\mathrm{m_h}} v_{\mathrm{d_h}} \Delta t (N_{\mathrm{t_h}} - n_{\mathrm{t_h}}) S_{\mathrm{h}}$. If those charges are all captured, the capturing rate could be found as (7).

Moreover, in terms of trapping cross-section S in (7), (S_{h} for holes or S_{e} for electrons), it has been pointed out that trapping cross-sectional area is corresponding to two factors: applied electric field [15] and trap depth [16].

In [15], an inverse power relationship between capture cross-section area and the average electric field has been found. Hence, we suppose in our model, if trap depth remains unchanged, the capture cross-section area S is proportional to $E^{-1.5}$ [15]. Moreover, estimated trapping parameters in [2, 3] imply that in dielectrics deeper traps should have a smaller cross-section area. Physically, it can be explained that smaller capture radius will give rise to a greater Coulombic-attractive force upon charge carrier, hence forming a deeper trap, which is harder for charge carrier to escape. Especially in [16], it was proposed that the binding energy W of a Coulombic trap to charge carrier is inversely proportional to radius of the trap r. The binding energy W directly determines the trap depth E_{t}. The larger W becomes, the tighter the charge carrier bounds to the trap, i.e. trap depth should be deeper. Here, it is assumed that E_{t} is proportional to W. Since trapping cross-sectional area $S = \pi r^2$, we could have S inversely proportional to E_{t}^2.

Thus, we introduced a capture cross-section area value S_0 at certain trap depth E_{t0} under electric field E_0, where in this paper, let $E_{\mathrm{t0}} = 1$ eV and $E_0 = 4 \times 10^7$ V/m. S_0 will be estimated by charge simulation curve fitting with experimental data. With such value S_0, trapping cross-sectional area S at any depth of E_{t} under electric field E ($<1.2 \times 10^8$ V/m) can be expressed as

$$S_{\mathrm{h}} = S_0 \left(\frac{E_{\mathrm{t0}}}{E'_{\mathrm{t_h}}}\right)^2 \left(\frac{E}{E_0}\right)^{-1.5} \tag{13}$$

With the averaged drift velocity v_{d}, the momentum p of the particle moving between two trap sites can be found as

$$p = m_{\mathrm{h,e}} v_{\mathrm{d}} = q E_{\pm} t_{\mathrm{d}} \tag{14}$$

where $m_{\mathrm{h,e}}$ is the effective mass of electrons or holes in material, $E_{\pm}$ is local electric field under effect of space charge accumulation in positive charge or negative charge region (same as E, but in different regions), t_{d} is time of the excited particle moving from one trap to the next. Ignoring Coulombic interactions and assuming the mobile charge is moving straight along the direction of local electric field (or reverse direction for mobile electrons) between trap sites, t_{d} can be expressed as: $t_{\mathrm{d}} = a/v_{\mathrm{d}}$, where a is trap separation distance. Hence, the averaged drift velocity of v_{d} can be expressed as

$$v_{\mathrm{d}} = \sqrt{\frac{q E_{\pm} a}{m_{\mathrm{h,e}}}} \tag{15}$$

Equation (8) gives the recombination rate of trapped positive charges with mobile electrons $n'_{\mathrm{m_e}} = \int_0^t \Delta n'_{\mathrm{m_e}} \, \mathrm{d}t$, in positive charge layer, which will reduce the trapped charge density in such charge layer.

Substituting the three terms in (5), a basic differential equation for the trapped charge amount dynamics in positive charge layer can be written as

$$\frac{\mathrm{d}n_{\mathrm{t_h}}}{\mathrm{d}t} = -n_{\mathrm{t_h}} \nu_0 \exp\left(-\frac{E'_{\mathrm{t_h}}}{kT}\right) + n_{\mathrm{m_h}} \left(N_{\mathrm{t_h}} - n_{\mathrm{t_h}}\right) S_{\mathrm{h}} v_{\mathrm{d_h}} - B\left(n'_{\mathrm{m_e}}\right) n_{\mathrm{t_h}} \tag{16}$$

Similarly, the equation for negative trapped charges can be developed.

2.1.2 Voltage-off condition: Moreover, in the depolarisation stage, charge carriers should move under field produced by local space charges. For the mobile carriers, the direction of movement should be dependent on the direction of local space charge field. Qualitatively, mobile positive charges near the anode will escape from adjacent electrode (anode), whereas those locating in the proximity of the other edge of the layer will flow to the opposite electrode (cathode). Again, without extraction barrier at both electrodes, we still assume a fix portion P_{h} of mobile charges will outflow from local charge region. Due to the removal of external voltage, as illustrated in Fig. 2, the charges in either charge layer will travel through bi-directionally dependent on the direction of local space charge field. In other words, only a portion of mobile charge loss will flow towards opposite electrode. For the sake of simplicity, it was assumed that charges are uniformly distributed in both charge layers and the zero-field locations in negative and positive charge layers are determined as x_- and x_+ and thickness of the sample is D. As calculated in [6], the values of x_- and x_+ are time variant, dependent on the induced charge and space charge density. Hence, mobile holes/electrons existing in positive/

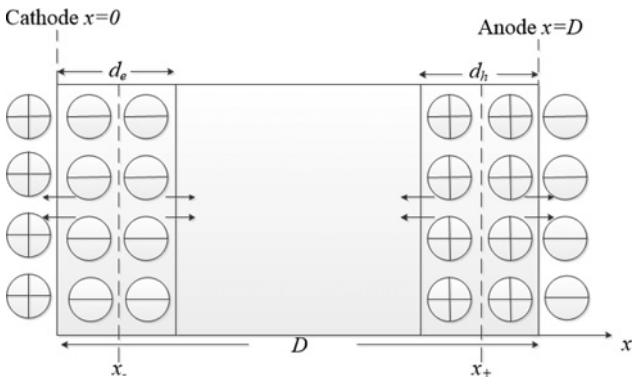

Fig. 2 *Charge distribution diagram after removal of external voltage*

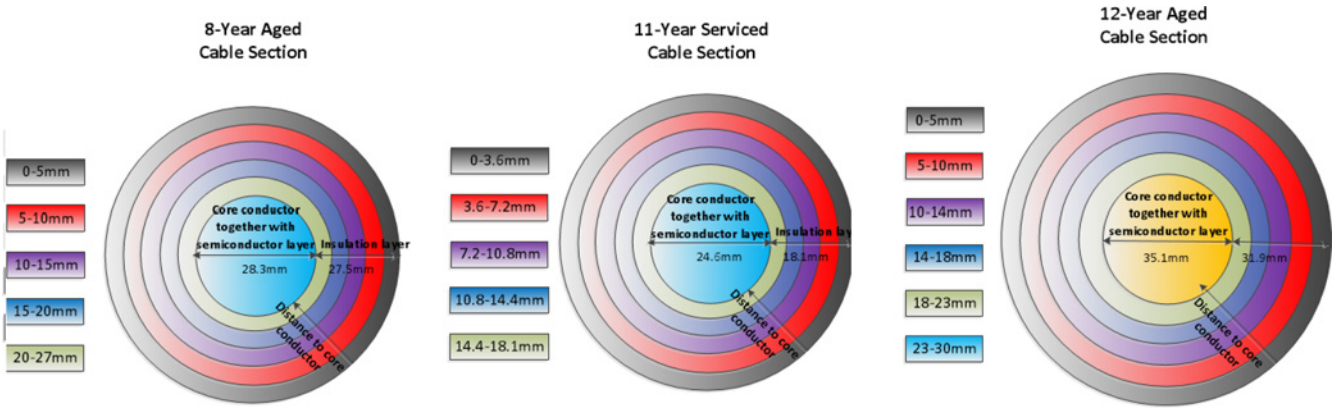

Fig. 3 *Cross-sections and grouping method on insulation layers of three different XLPE cables*

negative charge region during voltage-off condition can be found as shown in Fig. 2.

After the removal of external voltage, the Schottky injection at the metal–insulator interface could be neglected because electric field at electrodes E_i included within an exponential term is much lowered

(i) when $\left(1-\frac{x_-}{d_e}\right)P_e n_{m_e} > \left(1-\frac{D-x_+}{d_h}\right)P_h n_{m_h}$, $\Delta n'_{m_e} = \left(1-\frac{x_-}{d_e}\right)P_e n_{m_e} - \left(1-\frac{D-x_+}{d_h}\right)P_h n_{m_h}$ and $\Delta n'_{m_h} = 0$.

(ii) when $\left(1-\frac{x_-}{d_e}\right)P_e n_{m_e} < \left(1-\frac{D-x_+}{d_h}\right)P_h n_{m_h}$, $\Delta n'_{m_h} = \left(1-\frac{D-x_+}{d_h}\right)P_h n_{m_h} - \left(1-\frac{x_-}{d_e}\right)P_e n_{m_e}$ and $\Delta n'_{m_e} = 0$.

Hence, after removal of external voltage, the changing rate of net charge in positive region becomes

$$\frac{dn_h}{dt} = -P_h n_{m_h} - \Delta n'_{m_e} \tag{17}$$

In terms of the dynamic equation trapped charge during depolarisation stage, (16) will be suitable as well. However, the calculation of minority mobile electrons term $\Delta n'_{m_e}$ during depolarisation should consider the bi-directional flow of mobile charges. Moreover, values of field-dependent parameters need to be modified. These include Poole–Frenkel lowering ΔV_{pf_h}, and trapping cross-sectional area S_h. Full expressions and derivations of the averaged electric field at both voltage-on and voltage-off conditions and location of $x_\pm$ in either charge region are given in [6].

2.2 Based on dual energy level traps

In the improved single-level model, all traps in the polymeric material were presumed to be on the same energy level. Factually, these traps might exist within a range of levels in wide bandgap of insulation material. Typically, it was suggested that shallow and deep traps can be correlated with physical and chemical defects in the polymeric material, respectively [2, 3, 17, 18]. Physical defects can be created by changes in crystallinity, morphological structure and molecular weight, while chemical defects can be produced by oxidation and hydrolysis process [11, 18]. Hence, to assign the trapping parameters with more practical meaning, we extend the model from single level to dual energy levels.

With the model of dual levels, (3) becomes

$$\begin{aligned}\frac{dn_h}{dt} &= \frac{J_h}{qd_h} - P_h\, n_{m_h} - \Delta n'_{m_e} \\ &= \frac{J_h}{qd_h} - P_h\left(n - n_{t_{h1}} - n_{t_{h2}}\right) - \Delta n'_{m_e}\end{aligned} \tag{18}$$

where $n_{t_{h1}}$ and $n_{t_{h2}}$ represent the positive charges captured at shallow and deep energy level.

Based on (5)–(8), the changing rate of shallow trapped charges in positive charge layer could be expressed as

$$\frac{dn_{t_{h1}}}{dt} = -n_{t_{h1}}\nu_0 \exp\left(-\frac{E'_{t_{h1}}}{kT}\right) + n_{m_h}\left(N_{t_{h1}} - n_{t_{h1}}\right)S_{h1}v_{d_h} - Bn'_{m_e}n_{t_{h1}} \tag{19}$$

Likewise, for changing rate of deep trapped positive charges

$$\frac{dn_{t_{h2}}}{dt} = -n_{t_{h2}}\nu_0 \exp\left(-\frac{E'_{t_{h2}}}{kT}\right) + n_{m_h}\left(N_{t_{h2}} - n_{t_{h2}}\right)S_{h2}v_{d_h} - Bn'_{m_e}n_{t_{h2}} \tag{20}$$

where for hole traps at shallow and deep levels, respectively, $E'_{t_{h1}}$, $E'_{t_{h2}}$ are the modified trap depth, $\Delta V_{pf_{h1}}$, $\Delta V_{pf_{h2}}$ are the barrier height lowering due to Poole–Frenkel effect, S_{h1}, S_{h2} are the capturing cross-section area and v_{d_h} stands for the drift velocity of holes.

3 Sample preparation and experimental

XLPE cable sections were obtained from serviced high-voltage ac (HVAC) 220 kV cable systems (operated for 12 and 8 years) and also HVAC 110 kV cable system (operated for 11 years). The cable structure and the size are illustrated in Fig. 3. XLPE insulation was sliced to films by a rotary skiver (a cutting machine to make film by rotation) from the outer surface of cable insulation. The thickness of obtained samples was 145 ± 10 μm with smooth surface for space charge measurement and 100 ± 10 μm for dc breakdown test. To remove volatile chemicals in the film, the cut films were treated in vacuum oven at 80°C for 48 h for degassing [5].

The film samples for all the experiments were classified to several parts according to the distance from the surface of cable insulation as seen in Fig. 3. In this paper, for each cable, three different positions were selected as the outer, middle and inner layers according to the distance from the surface. Specific thickness range of each layer in three cable sections is given in Table 1.

The pulsed electroacoustic (PEA) technique was used for observing dynamics of charge profiles and measurements were made for 60 min after the removal of the applied voltage. For XLPE films with slightly different thickness, the applied voltage was adjusted so the applied field was fixed at 40 kV/mm for all the samples. The time of the applied voltage was 6 min. Moreover, for samples of each layer, three or four consecutive measurements

High Volt., 2016, Vol. 1, Iss. 2, pp. 95–105

Table 1 Grouping methods of three layers, respectively, for 8-, 11- and 12-year cable sections

Layers	Outer, mm	Middle, mm	Inner, mm
8-year	0–5.0	10.0–15.0	20.0–27.0
11-year	0–3.6	7.2–10.8	14.4–18.1
12-year	0–5.0	14.0–18.0	23.0–30.0

were made. Hence, charge amounts from each layer were averaged by those measured data.

From each layer, 15 samples of thinner thicknesses, (93 ± 10) μm, were used for dc breakdown tests. As was done with thicker samples for the PEA test, those samples were also processed with degassing treatment in vacuum oven at 80°C for 48 h. The prepared sample was tightly fixed between two sphere electrodes with a diameter of 6.5 mm. The external voltage was applied with a ramping rate of 100 V/s from zero. Moreover, in order to avoid flashover during test, the two spherical electrodes with the tested sample in between were immersed in insulating oil. For each type of sample, 15 measurements were made to reduce statistical error. To analyse the obtained breakdown data, the Weibull distribution has been used to describe their stochastic behaviours [19].

4 Charge results and discussion

In Figs. 4*a*–*i*, space charge dynamics of both voltage-on and voltage-off periods using inner-layer samples of were displayed. Figs. 4*a*, *d*, and *g* give the space charge dynamics during the voltage-on period.

To obtain the injected space charge profiles in the bulk, subtraction method was employed to eliminate the capacitive charges on two electrodes [20], as in Figs. 4*b*, *e* and *h*. Bipolar charges injection can be observed. After the removal of external voltage, the charge decay results are shown in Figs. 4*c*, *f* and *i*.

Charge amount in the positive charge layer could be found by the following equation

$$Q_{\mathrm{h}} = \int_{D-d_{\mathrm{h}}}^{D} \left| n_{\mathrm{h}}(x, t) q \right| A \, \mathrm{d}x \tag{19}$$

In the negative layer, it becomes

$$Q_{\mathrm{e}} = \int_{0}^{d_{\mathrm{e}}} \left| n_{\mathrm{e}}(x, t)(-q) \right| A \, \mathrm{d}x \tag{20}$$

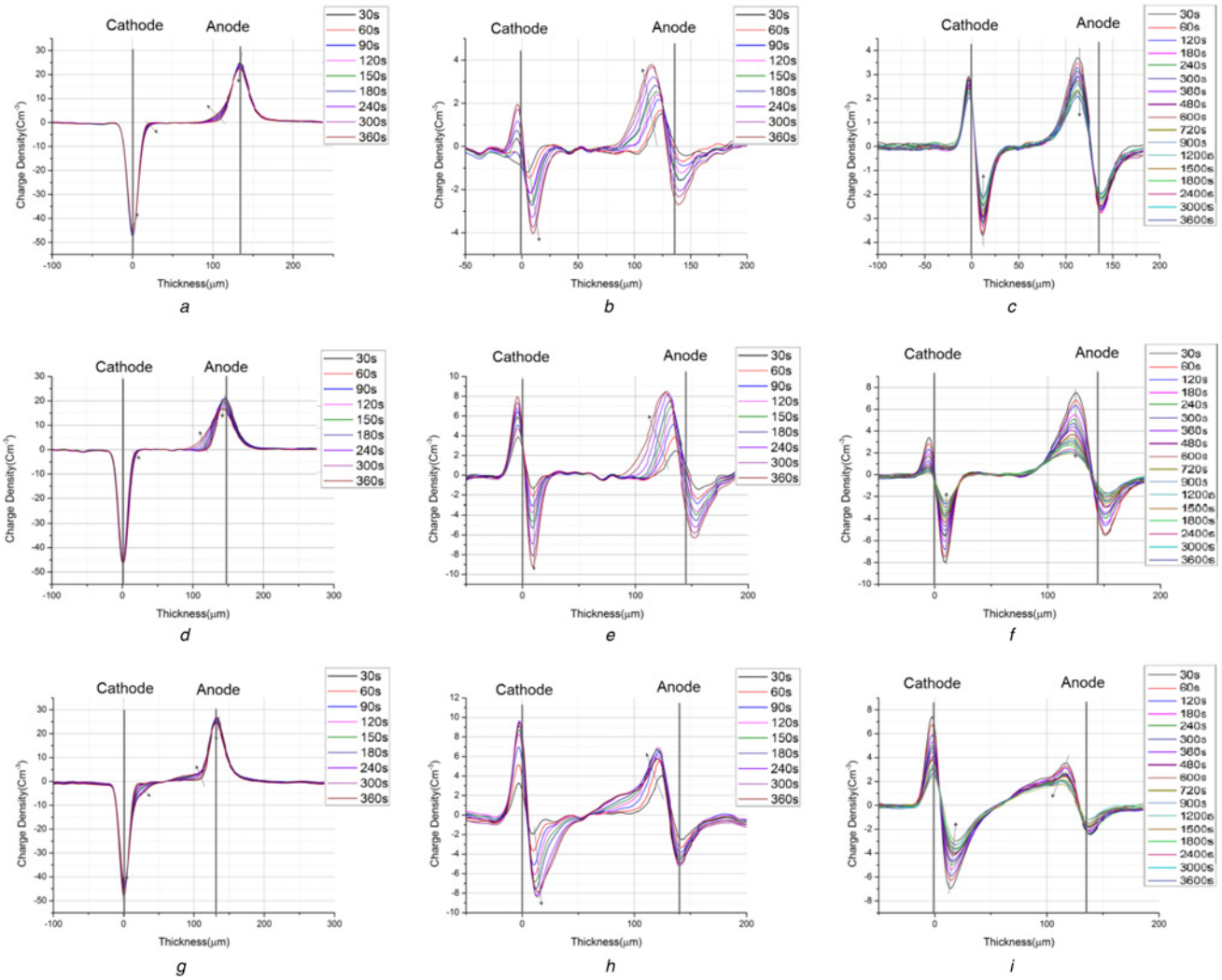

Fig. 4 *Space charge results of the inner-layer sample, respectively, for 12-year (a, b, c), 11-year (d, e, f), 8-year (g, h, i) cable section*

a, d, g Charge dynamics during voltage-stressing period of 6 min
b, e, h Charge dynamics during voltage-stressing period after subtraction algorithm
c, f, i Charge decay dynamic during depolarisation stage

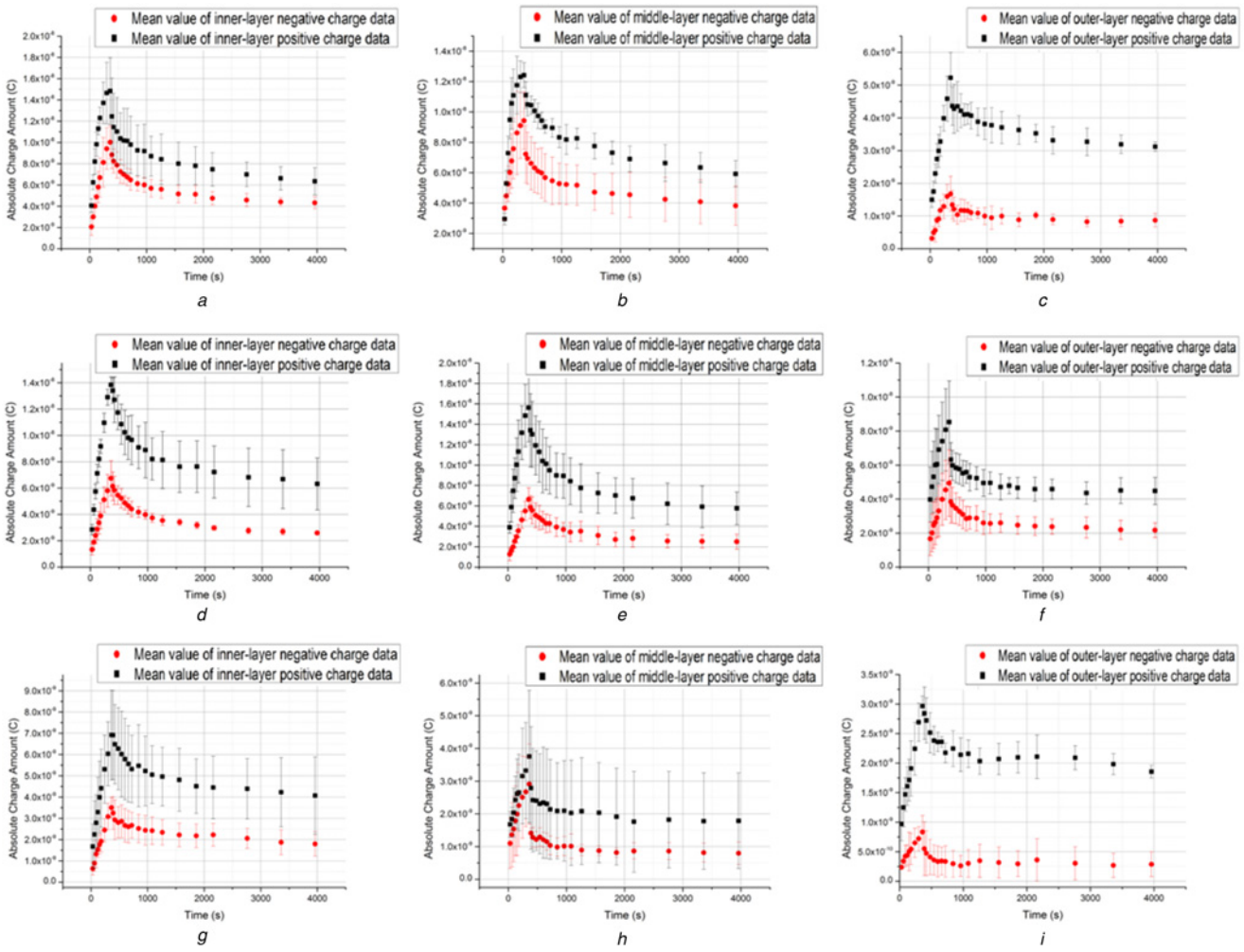

Fig. 5 *Averaged positive and negative charge amount of each layer samples, respectively, for*

a, b, c 12-year cable section
d, e, f 11-year cable section
g, h, i 8-year cable section
where (a, d, g): inner layer, (b, e, h): middle layer, (c, f, i): outer layer

With several measured data on each layer, charge amount of each charge layer can be averaged with error bars shown in Figs. 5*a–i*.

5 Simulation of charge amount by using dual energy level model

5.1 Model constants

In the present model, some parameters can be treated as constants in accordance with measured data or the previous literatures, values of which are shown in Table 2.

For thicknesses of positive and negative charge regions, i.e. d_e and d_h in the modelling, they are averaged from measured space charge profiles on number of PEA measurements. As the charge region also expands with time within the duration of voltage applying, we let d_e and d_h in calculation be the maximum expansion thickness with the time, as shown in Fig. 6, which is the charge profile of 11-year cable inner-layer samples. Specifically, for three layers of 12-, 11- and 8-year cable sections, averaged thicknesses of either space charge region are listed in Table 3.

5.2 Model parameters estimation

Since analytic solutions cannot be found for ordinary differential equations consisting of (18)–(20), the Euler method was carried out by supposing many small time steps Δt_s in the whole experimental time $t = 3960$ s. Therefore, we will have $(t/\Delta t_s) + 1$ points in the time space. For example, if we know the net positive

Table 2 Values of model constants

Model constant	Value
Q, C	1.60×10^{-19}
T, K	300
A_0, $Am^{-2}K^{-2}$	1.20×10^{6}
B, m^3s^{-1}[a]	6.40×10^{-19}
ϵ_0, Fm^{-1}	8.85×10^{-12}
K, JK^{-1}	1.38×10^{-23}
$m_{h,e}^*$, kg	9.11×10^{-31}
A, m^2	6.36×10^{-5}
v, s^{-1}[b]	2.00×10^{-13}
ϵ_r, Fm^{-1}	2.3

[a]Values from [9, 10].
[b]Values from [11].

High Volt., 2016, Vol. 1, Iss. 2, pp. 95–105

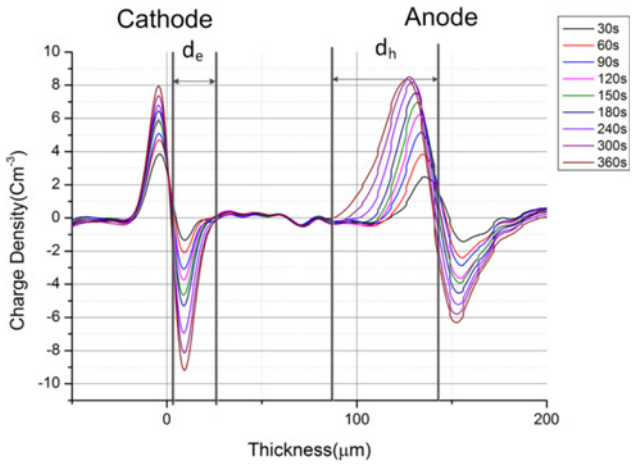

Fig. 6 *Charge profiles of 11-year inner-layer sample with external voltage applied in 360 s, demonstrating* d_e *and* d_h *during the charge region extension*

charge density at point i, i.e. $n_h(i)$, therefore $n_h(i+1)$ can be found by rewriting (3)

$$n_h(i+1) = n_h(i) + \Delta t\left[\frac{J_h(i)}{qd_h} - P_h(i)n_{m_h}(i) - \Delta n'_{m_e}(i)\right] \quad (21)$$

For the equation of trapped charge density in positive charge region, (16) can be rewritten in the form

$$n_{t_h}(i+1) = n_{t_h}(i) + \Delta t \left[-n_{t_h}(i)v_0\exp\left(-\frac{E'_{t_h}(i)}{kT}\right) + n_{m_h}(i)\left(N_{t_h} - n_{t_h}(i)\right) S_h(i)v_{d_h}(i) - B\left(n'_{m_e}(i)\right)n_{t_h}(i)\right] \quad (22)$$

Thus, the dynamic equations of n_e and n_{t_e} can be established in similar forms. Numerical solutions of $n_{h,e}$ and $n_{t_{h,e}}$ could be found one by one through MATLAB coding. In this paper, coefficients in these dynamic equations, e.g. reference trapping cross-sectional area S_0 (at 40 kV/mm, 1 eV), mobile charge escaping rate constant P, injection barrier w and trapping parameters, which include trap density N and depth E_t, have been set as unknown model parameters remaining to be estimated in the simulation.

In the program, nested 'for' loops consisting of all unknown model parameters within certain ranges were used to give many possible solutions. Referring to previous literatures [2, 3, 5, 9, 10], the ranges of injection barrier and trap depth can be assumed to be as: $1.100\ \text{eV} < w < 1.300\ \text{eV}$ and $0.900\ \text{eV} < E_t < 1.150\ \text{eV}$. In terms of trap density, it can be found that from previous works around order of $10^{19}\ \text{m}^{-3}$. Therefore, the initial density of shallow and deep traps should be initially tried around that value, for example, from 1×10^{18} to $1 \times 10^{21}\ \text{m}^{-3}$. In terms of the escaping rate of percentage, it is hard to be determined as this is a new parameter proposed in the paper. We assumed that $0.001\ \text{s}^{-1} < P < 0.010\ \text{s}^{-1}$. To sum up, these parameters' ranges of our first program run can be listed as in Table 4. If the optimum values of one or more parameters were found at upper or lower boundary of the ranges, we will extend the initial ranges accordingly and re-run the program for another group of optimum values. Finally, a group of optimum model parameters can be found within or slightly outside the initial ranges set up in Table 4. However, the model parameters obtained by such approach might not be the best solution. The global optimum values perhaps occur at several orders different from the initial ranges of Table 4, but these values does not have any physical meanings as they are quite not consistent with the values of parameters found in many previous researches [2, 3, 5, 9, 10].

For the value of reference cross-section area S_0, it is supposed to be a constant value as the field and trap depth are confirmed. However, we lack the evidence of specific value of S_0 from previous literatures. Hence, another approach has to be developed to estimate the value of S_0. One possible way is to put S_0 into certain range and find the value of best fitting. Actually, this is not feasible since S_0, which is considered to be a constant at certain field and trap depth, will be obtained as different values by fitting with different curves of different type of samples. However, this process still gives the value S_0 around the order of $10^{-30}\ \text{m}^2$. Thus, we assumed that S_0 equal to $1.00 \times 10^{-30}\ \text{m}^2$ for both electrons and holes.

In some previous literature [1–3, 9, 10], many literatures pointed out that cross-section area should be values around 10^{-18}–$10^{-16}\ \text{m}^2$. The big difference can be explained by three reasons. (i) Those larger values of cross-section area are measured at voltage-off condition, implying much smaller local electric field than 40 kV/mm, thus a much larger cross-section area.(ii) In the present model, mobile charges and trapped charges are separated. However, in the model of [1–3], any displayed charges are considered to be trapped charges. This will give rise to enhancement of trapping ability of the material, i.e. large cross-section area. (iii) The most important reason is that different theories were applied to the equation to calculate charge capturing rate, which includes the term of trapping cross-section area. By comparing the equations about charge capturing rate in [1–3] with (8) about R_{cap} in the present article, it can be found that the product of charge drift velocity traveling between traps (v_d) and mobile charge density (n_m) was simply replaced by the term of metal–insulator interface current density J. Hence, the trapping cross-section area values calculated in [1–3] give more information on trapping ability of material near surface. In the present model, we are targeting to estimate the overall trapping ability in the sample bulk.

Through iterative process, these parameters for each set of data can be estimated by finding the best curve fitting output between experimental data and many numerical solutions, i.e. highest R-square value. The R-square is the square of the correlation between the response values and the predicted response values. With a value closer to 1, it indicates that a greater proportion of variance is accounted for by the model.

The highest R-square values for three different cable sections were determined in Table 5. However, the fitting is not so good (from

Table 4 Initial ranges of unknown model parameters

Parameters	Min	Max
P, s^{-1}	0.001	0.010
w, eV	1.100	1.300
E_t, eV	0.900	1.150
	0.900	1.150
N_t, m^{-3}	1×10^{18}	1×10^{21}

Table 3 Averaged thickness of either space charge region

Layers		Outer, μm	Middle, μm	Inner, μm
12-year	d_e	36	25	16
	d_h	58	36	40
11-year	d_e	30	23	25
	d_h	70	68	42
8-year	d_e	41	57	21
	d_h	80	77	43

Table 5 Obtained R-square values of three layers, respectively, for 12-, 11- and 8-year-operated cable sections

Layers	Inner	Middle	Outer
12-year	0.974	0.880	0.927
11-year	0.974	0.935	0.845
8-year	0.973	0.963	0.978

Table 6 Estimated parameters (electrons and holes) of three layers, respectively, for 12-, 11- and 8-year-operated cable sections, using dual level modelling, where in the table 'S' and 'D' stands for trapping parameters at shallow and deep level, respectively

Parameters		Electrons	Holes
12-year cable		Inner layer	
P, s^{-1}		0.004	0.002
w, eV		1.204	1.184
E_t, eV	S	0.965	0.974
	D	1.019	1.042
N_t, m^{-3}	S	1.32×10^{19}	8.71×10^{20}
	D	1.51×10^{19}	8.08×10^{20}
		Middle layer	
P, s^{-1}		0.006	0.004
w, eV		1.200	1.192
E_t, eV	S	1.023	1.023
	D	1.083	1.076
N_t, m^{-3}	S	1.84×10^{19}	6.91×10^{20}
	D	3.33×10^{18}	8.14×10^{20}
		Outer layer	
P, s^{-1}		0.007	0.001
w, eV		1.233	1.202
E_t, eV	S	1.019	1.030
	D	1.091	1.086
N_t, m^{-3}	S	2.24×10^{18}	6.33×10^{20}
	D	1.36×10^{18}	7.64×10^{20}
11-year cable		Inner layer	
P, s^{-1}		0.003	0.003
w, eV		1.190	1.161
E_t, eV	S	0.912	1.015
	D	1.004	1.092
N_t, m^{-3}	S	5.13×10^{19}	2.31×10^{21}
	D	4.22×10^{19}	1.58×10^{21}
		Middle layer	
P, s^{-1}		0.004	0.003
w, eV		1.187	1.149
E_t, eV	S	0.916	0.985
	D	0.989	1.030
N_t, m^{-3}	S	6.11×10^{19}	3.47×10^{21}
	D	4.34×10^{19}	2.12×10^{21}
		Outer layer	
P, s^{-1}		0.004	0.003
w, eV		1.193	1.175
E_t, eV	S	1.012	1.018
	D	1.117	1.083
N_t, m^{-3}	S	1.84×10^{19}	4.54×10^{20}
	D	4.56×10^{19}	1.03×10^{21}
8-year cable		Inner layer	
P, s^{-1}		0.005	0.002
w, eV		1.170	1.149
E_t, eV	S	0.958	0.982
	D	1.034	1.041
N_t, m^{-3}	S	7.21×10^{19}	1.72×10^{21}
	D	5.72×10^{19}	9.82×10^{20}
		Middle layer	
P, s^{-1}		0.005	0.002
w, eV		1.170	1.158
E_t, eV	S	0.972	0.973
	D	1.048	1.011
N_t, m^{-3}	S	2.80×10^{19}	9.81×10^{20}
	D	4.07×10^{19}	8.08×10^{20}
		Outer layer	
P, s^{-1}		0.006	0.005
w, eV		1.216	1.188
E_t, eV	S	1.021	1.025
	D	1.109	1.070
N_t, m^{-3}	S	1.81×10^{18}	7.58×10^{20}
	D	4.63×10^{18}	6.12×10^{20}

0.845 to 0.974). This can be explained by two reasons. (i) For each type of samples, best fitting result was produced by considering optimisation of two curves as parameters of both electrons and holes are nested with each other. (ii) One uncertain value, S_0 was assumed to be a constant before fitting. This can affect the result as well since such value (1.00×10^{-30} m^2) might not be the optimum solution. Thus, unknown parameters can be estimated, as shown in Table 6.

For example of inner-layer samples, through the simulation process based on our improved model, the fitting curves can be obtained, as shown in Figs. 7*a–c*. In such figure, it is noteworthy that when the applied voltage is switched off, mobile charges start to reduce in each charge layer while trapped charges continue increasing to certain amount then fall (for shallow trapped charges) or almost keep flat (for deep trapped charges). This can be attributed to the trapping cross-section area enlargement after the removal of external voltage, i.e. under much weaker field. Thereafter, a number of mobile charges get retrapped into empty sites. However, as the rapid decrease of mobile charges to nearly zero, little charges can be caught into trapped sites and detrapping process become predominating in the bulk.

6 DC breakdown test

For these experiments, the prepared sample was tightly fixed between two sphere electrodes with diameter of 6.5 mm. The external voltage was applied as ramping voltage stepping with 100 V/s from zero. Moreover, in order to avoid flashover during test, the two spherical electrodes with the tested sample in between were immersed in insulating oil. For each type of sample, around 15 measurements were made to reduce statistical error.

To analyse obtained breakdown data, the Weibull distribution has been found to be a most appropriate approach to describe their stochastic behaviours. Figs. 8*a–c* show the Weibull plotting of dc breakdown voltage, respectively, for 12-, 11- and 8-year XLPE cable peelings, respectively. The breakdown strengths for all types of sample determined by the Weibull distribution can be found in Table 7. Within 95% confidence bounds, upper and lower bounds at a characteristic value that breakdown probability equals to 63.2% (irrespective of shape factor of Weibull distribution) are also listed in Table 7.

7 Analysis

From Table 6, it can be summarised that for each layer of three different XLPE cable sections, the injection barrier of holes is generally lower than that of electrons. This indicates, for XLPE films, holes can inject into the sample more easily than electrons.

In terms of trapping parameters, trap density are calculated at two separated energy levels, as shown in Table 6. As discussed in Section 5.2, trapped charges at both levels manifest different charge dynamics at depolarisation stage. In Fig. 7, after around 500 s, shallow trapped charges slowly decrease to certain low level whereas deep trapped charges still stay at a higher level. After 2500 s, the remaining charges in sample bulk are mainly deep trapped charges.

7.1 Breakdown strengths versus service condition

From Table 7, for all three cable sections, the dc breakdown performance of outer-layer samples is most superior to the other two layers. Specifically for 12- and 8-year operated cable (serviced at HVAC 220 kV), the breakdown strength of inner layer is lower than that of middle layer, whereas for 11-year operated cable (serviced at HVAC 110 kV), the breakdown strength of inner layer is higher.

Without considering space charge issues, the dependence on electric field can be found in (21), which is suitable for cylindrical

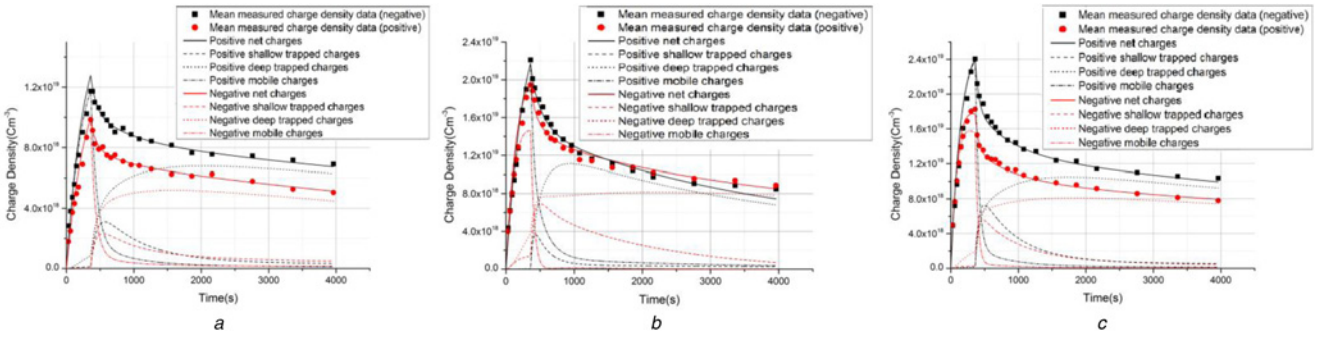

Fig. 7 *Simulated curves fitting with experimental data of inner-layer samples, respectively, for*

a 12-year operated cable peelings
b 11-year operated cable peelings
c 8-year operated cable peelings, based on dual-energy level model

insulation cable of one material at ac condition [21]

$$E(r) = \frac{U}{r\ln(R_o/R_i)} \tag{21}$$

where U stands for the applied voltage, r is the distance from the centre of core conductor, R_o is external radius of the insulation and R_i is the radius of core conductor.

Considering the diameters of core conductor illustrated in Fig. 3, we can have electric field ranges calculated for each layer of three

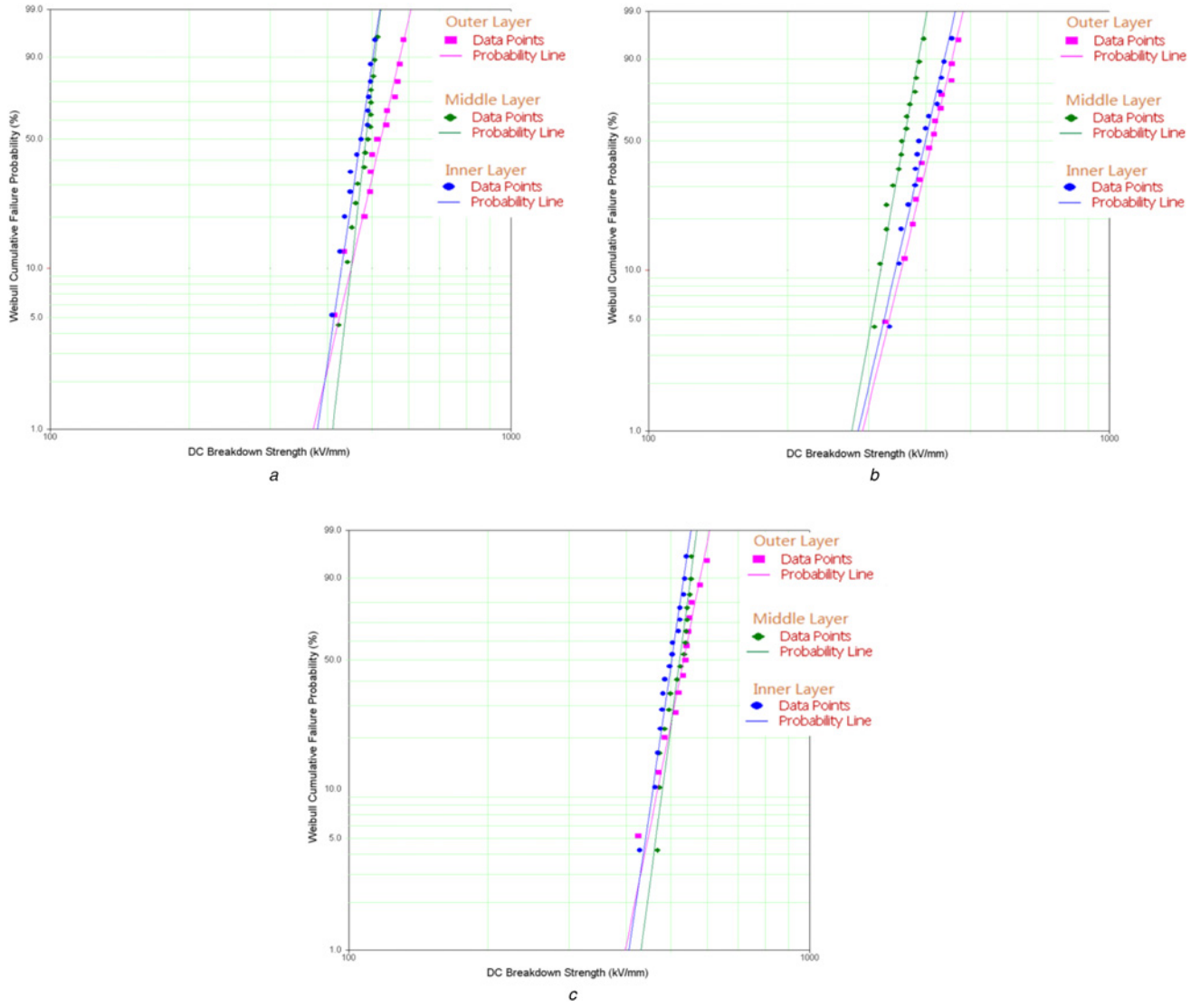

Fig. 8 *Weibull plot of the cumulative probability of breakdown versus breakdown voltages of three layers, respectively, for*

a 12-year operated cable peelings
b 11-year operated cable peelings
c 8-year operated cable peelings

Table 7 Breakdown strengths for each layer of XLPE films within 95% confidence bounds at unreliability = 63.2%

Types of XLPE films	Lower bound (95%), kV ·mm^{-1}	Breakdown strength, kV mm^{-1}	Upper Bound (95%), kV mm^{-1}
12-year inner	464.91	480.49	495.51
12-year middle	479.50	490.75	501.56
12-year outer	510.23	537.08	563.49
11-year inner	391.31	410.06	428.44
11-year middle	352.67	365.66	378.26
11-year outer	404.00	424.95	445.59
8-year inner	496.51	510.94	524.86
8-year middle	517.06	530.80	543.97
8-year outer	522.53	545.99	567.07

Table 8 Operation electric field range in different layers of XLPE cable peelings, respectively, for three cable sections

Cable type	Electric field, kV mm^{-1}		
	Outer layer	Middle layer	Inner layer
12-year cable	4.29–4.76	5.96–6.74	8.02–10.90
11-year cable	4.00–4.55	5.26–6.23	7.65–9.88
8-year cable	4.89–5.52	6.45–7.62	9.39–13.89

cable sections in Table 8. According to the table, the insulation status in 12- and 8-year cable sections can be easily explained by the operation electric field distribution through the radial direction through the cable section. Nevertheless, in the 11-year cable section, the worst breakdown strength performance of the middle-layer samples cannot be elucidated by the operation field distribution at HVAC condition. Instead, the situation might be explained by the space charge issues.

In this paper, an ac test was run on a XLPE slice from 12-year cable peelings. The PEA measurement was accomplished under electric field applied at 35 kV/mm within 47 h. From Figs. 9*a* and *b*, a considerable positive charge expansion can be observed from the top electrode (adhered by semi-conductive layer) meanwhile a little negative injection can also be observed near the ground electrode (aluminium). Fig. 9*c* gives the voltage-off charge profile just after removal of the external ac voltage and directly shows space charge distribution in the sample, which is consistent with that measured during voltage-on period. Hence, we might make a conjecture that, compared with electrons, holes are more easy to inject into the XLPE insulation layer through the metal-semiconductor interface. Such interface happens to be the same case with extruded cable insulation structure, which contains inner and outer semiconducting layers for shielding purposes. Therefore, after long-term operation under HVAC condition of many years, positive charges might gradually accumulate in the vicinity of both inner and outer insulation regions. These charges could distort the internal field distribution through the radial direction. In this paper, as the 11-year cable section was operated under service condition of 110 kV, the cable system was designed to be smaller. With smaller scale of the cable, the severe impact of space charges will be made. This might explain the worst dc breakdown performance of middle layer from 11-year cable section.

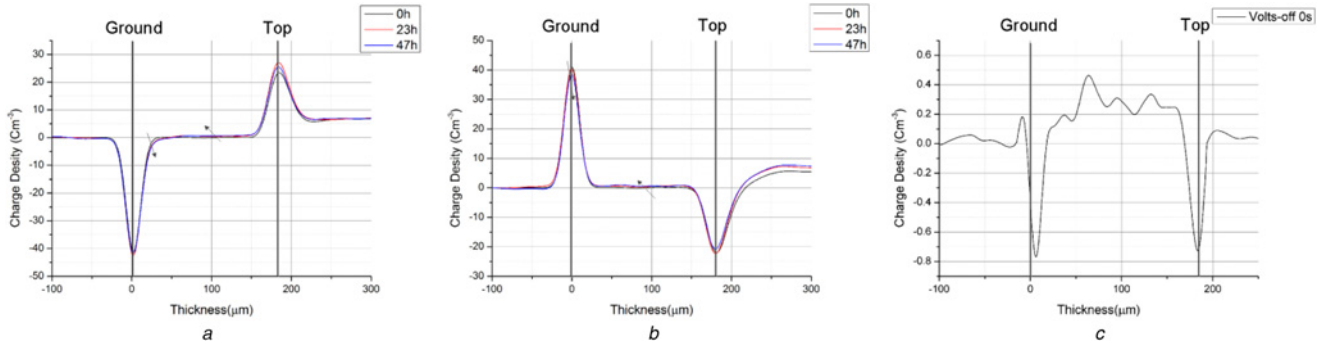

Fig. 9 *Space charge measurement on a virgin XLPE peeling of 180 μm from 12-year serviced cable section under the ac condition of 35 kV/mm within 47 h*

a At 90°, positive peak
b At 270°, negative peak
c 0 h after removal of the external voltage

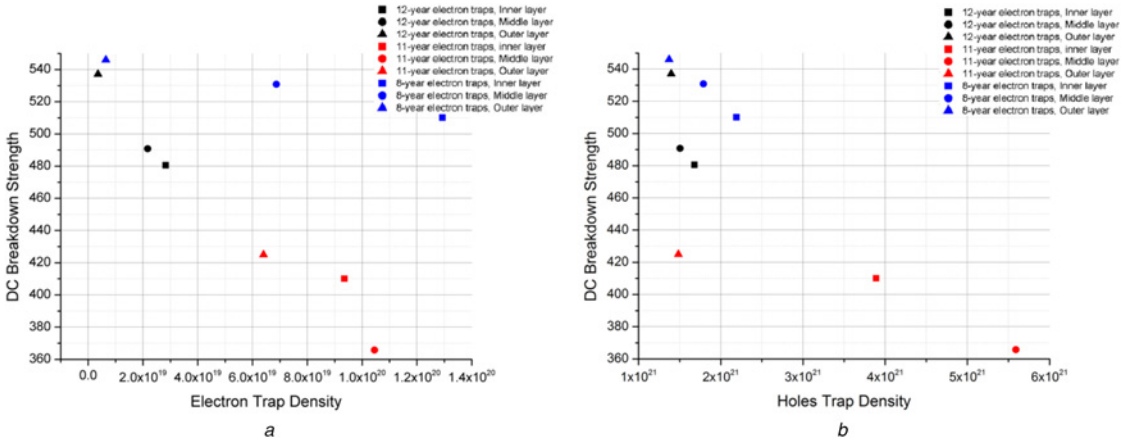

Fig. 10 *Plotting of trap density estimated for different samples versus their dc breakdown strengths*

High Volt., 2016, Vol. 1, Iss. 2, pp. 95–105

Table 9 Averaged trap depth calculated for different layers of XLPE cable peelings, respectively, for three cable sections

Cable type		Inner	Middle	Outer
12-year	electrons, eV	0.994	1.032	1.046
	holes, eV	1.007	1.052	1.061
11-year	electrons, eV	0.954	0.946	1.087
	holes, eV	1.046	1.002	1.063
8-year	electrons, eV	0.992	1.017	1.084
	holes, eV	1.003	0.990	1.045

7.2 Breakdown strength versus trapping parameters

Since injection barrier will determine the initial charge density at metal (semiconductor)–insulator layer under HV, it should be tightly correlated with the breakdown performance of the material. With both Tables 6 and 7, it can be found that, in the same cable, with lower injection barrier of the sample (either holes or electrons), i.e. more free charges will be initially injected into the insulation system, the dc breakdown strength generally become lower.

If we relate the total trap density for electrons and holes, i.e. sum of shallow and deep trap density, with dc breakdown strength of each type of samples, the correspondence can be summarised as in Fig. 10. From both Figs. 10*a* and *b*, it can be concluded that: in the same cable section, with the increase of trap density, the dc breakdown strength goes lower. This can be explained by the reason that the higher trap density might imply more physical and chemical defects existing in the sample, i.e. the material was more severely aged. More specifically, with more traps in the material, trapping ability can be enhanced, which give rise to a larger field distortion caused by more space charge accumulated in the sample.

Moreover, an averaged trap depth $\overline{E_t}$ can be calculated for each type of samples as in the following equation:

$$\overline{E_t} = \frac{N_{t_1} E_{t_1} + N_{t_2} E_{t_2}}{N_{t_1} + N_{t_2}} \tag{22}$$

Comparing Table 9 with breakdown data in Table 7, it can be found that generally with shallower trap depth, the breakdown strength become lower. In light of the detrapping (6), shallower trap depth will lead to faster get-away of trapped charges from the localised states. Hence, more mobile charges will contribute to the formation of a higher current density in the polymeric material.

8 Conclusion

In this paper, an improved trapping/detrapping model was employed to simulate both the trapped and mobile charge amount dynamics of different XLPE peelings from different layers of three cable sections taken from service conditions.

Furthermore, for each type of samples, injection barrier and trapping parameters were estimated through the model. Relating the estimated parameters with dc breakdown performance of each type of samples in the same cable, it can be found that the rule that with the lower injection barrier, higher trap density or shallower overall trap depth, the dc breakdown performance become worse. In other words, these parameters obtained from the model might be utilised as a diagnostic tool to monitor the insulation status in the cable system. More specifically, model parameters of seriously-aged or failed polymeric cable materials can be calculated as reference values for the same cable materials in normal operation. If the estimated parameters of certain part from normally-operating cable are similar with reference values, it should indicate the upcoming failure of the material.

9 Acknowledgment

The authors are grateful for the financial support from the State Grid Cooperation of China: Research on Key Technologies of Insulation Material and Accessories for 320 kV HVDC XLPE Cable System (SGRIZLJS(2014)888).

10 References

1 Chen, G., Xu, Z.: 'Charge trapping and detrapping in polymeric materials', *J. Appl. Phys.*, 2009, **106**, p. 123707
2 Zhou, T., Chen, G., Liao, R., *et al.*: 'Charge trapping and detrapping in polymeric materials: trapping parameters', *J. Appl. Phys.*, 2011, **110**, p. 043724
3 Liu, N., Chen, G.: 'Changes in charge trapping/detrapping in polymeric materials and its relation with aging'. Conf. on Electrical Insulation and Dielectric Phenomena, Annual Report, 2013, pp. 800–803
4 Dissado, L., Griseri, V., Peasgood, W., *et al.*: 'Decay of space charge in a glassy epoxy resin following voltage removal', *IEEE Trans. Dielectr. Electr. Insul.*, 2006, **13**, (4), pp. 903–916
5 Tzimas, A., Rowland, S., Dissado, L.: 'Effect of electrical and thermal stressing on charge traps in XLPE cable insulation', *IEEE Trans. Dielectr. Electr. Insul*, 2012, **19**, (6), pp. 2145–2154
6 Liu, N., He, M., Alghamdi, H., *et al.*: 'An improved model to estimate trapping parameters in polymeric materials and its application on normal and aged low-density polyethylenes', *J. Appl. Phys.*, 2015, **118**, p. 064102
7 Brunson, J.: 'Hopping conductivity and charge transport in low density polyethylene'. PhD thesis, Utah State University, 2010
8 Miyoshi, Y., Chino, K.: 'Electrical properties of polyethylene single crystals', *Jpn. J. Appl. Phys.*, 1967, **6**, (2), pp. 181–190
9 Roy, S., Segur, P., Teyssedre, G., *et al.*: 'Description of bipolar charge transport in polyethylene using a fluid model with a constant mobility: model prediction', *J. Appl. Phys. D, Appl. Phys.*, 2004, **37**, (2), pp. 298–305
10 Zhao, J.: 'Dynamics of space charge and electroluminescence modelling in polyethylene'. PhD thesis, University of Southampton, 2011
11 Dissado, L., Fothergill, J.: 'Deterministic mechanisms of breakdown' in Stevens, G. (ed): 'Electrical degradation and breakdown in polymers' (Peters Peregrinus Ltd., London, United Kingdom, 1992, 9th edn.)
12 Nath, R., Kaura, T., Perlman, M.: 'Steady-state conduction in linear low-density polyethylene with Poole-lowered trap depth', *IEEE Trans. Dielectr. Electr. Insul.*, 1990, **25**, (2), pp. 419–425
13 Raju, G.: 'Dielectrics in electric fields' (Marcel Dekker, Inc., New York, United States, 2003)
14 Ieda, M., Sawa, G., Kato, S.: 'A consideration of Poole–Frenkel effect on electric conduction in insulators', *J. Appl. Phys.*, 1971, **42**, (10), pp. 3737–3740
15 Buchanan, D., Fischetti, M., DiMaria, D.: 'Coulombic and neutral trapping centers in silicon dioxide', *Phys. Rev. B*, 1991, **43**, (2), pp. 1471–1486
16 Blaise, G., Sarjeant, W.: 'Space charge in dielectrics. Energy storage and transfer dynamics from atomistic to macroscopic scale', *IEEE Trans. Dielectr. Electr. Insul.*, 1998, **5**, (5), pp. 779–808
17 Mazzanti, G., Marzinotto, M.: 'Extruded cables for high voltage direct current transmission: advances in research and development' (John Wiley and Sons, New Jersey, United States, 2013)
18 Marsacq, D., Hourquebie, P., Olmedo, L., *et al.*: 'Effects of physical and chemical defects of polyethylene on space charge behaviour'. Conf. on Electrical Insulation and Dielectric Phenomena, Annual Report, 1995, pp. 672–675
19 Khalil, M.S.: 'The role of BaTiO3 in modifying the dc breakdown strength of LDPE', *IEEE Trans. Dielectr. Electr. Insul.*, 2000, **7**, (2), pp. 261–268
20 Liu, N., Zhou, C., Chen, G., *et al.*: 'Determination of threshold electric field for charge injection in polymeric materials', *Appl. Phys. Lett.*, 2015, **106**, p. 192901
21 Jeroense, M., Morshuis, P.: 'Electric fields in HVDC paper-insulated cables', *IEEE Trans. Dielectr. Electr. Insul.*, 1998, **5**, (2), pp. 225–236